Nuclear Materials and Energy 41 (2024) 101803

Contents lists available at ScienceDirect

Nuclear Materials and Energy

journal homepage: www.elsevier.com/locate/nme

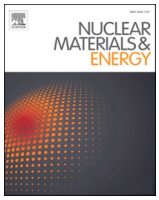

Full-torus impurity transport simulation in boron powder injection experiments in the Large Helical Device

M. Shoji [a,b,*], G. Kawamura [a,c], R. Smirnov [d], J. Romazanov [e], A. Kirschner [e], Y. Tanaka [f], S. Masuzaki [a,b], T. Kawate [a,b], F. Nespoli [g], R. Lunsford [g], E.P. Gilson [g], S. Brezinsek [e], N.A. Pablant [g]

[a] National Institute for Fusion Science, National Institutes of Natural Sciences, Oroshi-cho, Toki, Gifu 509-5292 Japan
[b] The Graduate University for Advanced Studies (SOKENDAI), Shonan Village, Hayama, Kanagawa 240-0913, Japan
[c] National Institutes for Quantum Science and Technology, Rokkasyo Institute for Fusion Energy, Rokkasho-mura, Aomori 039-3212, Japan
[d] Department of Mechanical and Aerospace Engineering, University of California at San Diego, La Jolla, CA 92093, USA
[e] Forschungszentrum Jülich GmbH, Institut für Energie- und Klimaforschung - Plasmaphysik, Partner of the Trilateral Euregio Cluster (TEC), Jülich 52425, Germany
[f] Institute of Science and Engineering, Kanazawa University, Kakuma, Kanazawa 920-1192, Japan
[g] Princeton Plasma Physics Laboratory, 100 Stellarator Road, Princeton, NJ 08540, USA

ARTICLE INFO

Keywords:
Impurity powder dropper
ERO2.0
DUSTT
EMC3-EIRENE
LHD
Boronization

ABSTRACT

The toroidal distribution of boron deposition on plasma-facing components (PFCs) in boron powder injection using an impurity power dropper (IPD) was investigated by full-torus simulation and observations in a systematic plasma density-scan experiment. The images of the ablation of dropped boron powders observed with a visible CCD camera were consistently explained by the simulations of the ablation positions of the boron powders considering the size distribution. Simulations assuming full-torus boron deposition on the PFCs did not reproduce the observed intensity profile of boron emission lines for higher plasma densities. It indicated that the density of boron deposited on PFCs installed toroidally far from the IPD was low for higher plasma densities due to the change in the ablation positions of the boron powders toward the outboard side. The experimental results verified the previous full-torus simulation of the toroidal distribution of the boron deposition in both lower and higher plasma densities.

Introduction

The Impurity Powder Dropper (IPD) has gotten attention as an alternative method for effective wall conditioning, such as real-time boronization which can be performed without plasma discharge interruption and with magnetic field excitation [1–5]. The real-time boronization is realized by injecting boron powders into the plasma discharges, which has several advantages over conventional wall-conditioning such as glow-discharge cleaning (GDC), using diborane (B_2H_6) gases [6,7]. In the Large Helical Device (LHD) [8], an IPD was installed in the upper port (2.5-U) to inject impurity powders into the plasma to investigate the effect of the boronization, impurity transport, and plasma confinement [9]. In the divertor configuration in LHD, real-time boronization seems preferable for forming boron-deposition layers on the divertor plates in a closed helical diverter region to the GDC. This is because the divertor plates do not directly face the main plasma and the divertor region is enclosed by the plates, preventing the formation of boron deposition layers on the divertor plates by the GDC. Meanwhile, one of the main concerns of real-time boronization is the toroidal uniformity of the distribution of the boron deposition layers on the plasma-facing components (PFCs) because the IPD is installed at only one of the upper ports at a toroidal position in the torus. Thus, the analysis of the full-torus impurity (boron) transport and the boron density profile deposited on the PFCs is essential for using the IPD as a tool for wall-conditioning. The impurity transport in real-time boronization is affected by the position and the spatial distribution of the impurity source in the peripheral plasma produced by the ablation of dropped impurity powders.

In LHD, simulation analyses using a dust transport code (DUSTT) [10–12] and a three-dimensional edge plasma code (EMC3-EIRENE) [13–16] revealed that the trajectories and ablation positions of the dropped impurity powders strongly depended on the plasma density

* Corresponding author.
E-mail address: shohji.mamoru@nifs.ac.jp (M. Shoji).

https://doi.org/10.1016/j.nme.2024.101803
Received 18 June 2024; Received in revised form 6 October 2024; Accepted 31 October 2024
Available online 4 November 2024

[17]. Boron powders dropped from the IPD must pass through an upper divertor leg before reaching the peripheral plasma (the ergodic layer). The powders were evaporated by the heat load from the plasma, resulting in the ablation of the boron powders and the production of atomic boron sources in the plasma. The simulation showed that the ablation position changed toward the outboard side of the torus with the increase in the plasma density. This is because the trajectory of the boron powders is deflected by the effect of the plasma flow in the upper divertor leg [17]. Considering the deflection of the trajectories, the IPD was installed at an optimized position on an upper port, which contributed to the improvement of the energy confinement in LHD plasmas [18]. The boron powders dropped from the optimized position passed through the divertor leg and the powders successfully reached the ergodic layer to supply boron ions in the peripheral plasma. Simulation analyses using the three-dimensional plasma surface interaction (PSI) code (ERO2.0) [19,20] predicted that the change in the ablation positions for higher plasma densities brought a localized distribution of the boron deposition in a toroidal section adjacent to the IPD [21]. This is because the connection lengths of the magnetic field lines are short at the ablation positions in the outer edge of the ergodic layer. The magnetic field lines with shorter connection lengths directly connect to the PFCs near the ablation positions underneath the IPD.

To verify the prediction of the full-torus simulation, a boron powder injection experiment was performed with a systematic scan of the plasma density. In the following section, the calculations of the trajectories of the boron powders are shown, which were performed to find an optimized position of the IPD. In section 3, the dust transport simulation code is applied to the analysis of the observed ablation images of the dropped boron powders. In section 4, the intensity profile of boron emission lines measured with a visible spectrometer array is investigated using the full-torus simulation.

Optimization of the position of the impurity powder dropper

In LHD, a helically twisted plasma with poloidal/toroidal period numbers of 2/10 is formed by the magnetic field produced by external super-conducting helical and poloidal coils [8]. Four bundled magnetic field lines deviate from X-points in the ergodic layer, which are called divertor legs. The trajectory of boron powders dropped from the IPD is deflected by the effect of the plasma flow in the upper divertor legs [17], which can disturb the injection of boron powders into the plasma. We had four candidate positions for installing the IPD on the upper port (2.5-U). The analysis by the dust transport simulation was applied to find an optimized position to inject the powders into the plasma as deep as possible. The deep penetration of the boron powders is advantageous in achieving more toroidally uniform boron deposition on the divertor plates [21]. Fig. 1 displays the calculated trajectories of dropped boron powders under three-dimensional background hydrogen plasmas calculated by EMC3-EIRENE, in which the plasma density inside the Last Closed Flux Surface (LCFS), n_e^{LCFS}, was changed from 1×10^{19} m^{-3} to 6×10^{19} m^{-3} with a fixed plasma heating power inside the LCFS, P^{LCFS}, of 8 MW and the radial position of the magnetic axis in the major radius, R_{ax}, was 3.60 m which is the most typical magnetic configuration in plasma discharge operation in LHD. Particle and heat transport coefficients in the plasma were set to 0.5 m^2/s and 1.0 m^2/s, respectively, which are typical values for reproducing the plasma parameter profiles. No impurities are included in the background plasma for simple calculation. Boron powders with a diameter of 150 μm were dropped by gravity from the points vertically underneath the four candidate positions with an initial downward velocity of 5 m/s. The diameter is the nominal one used in the boron powder injection experiments. The downward velocity corresponds to the speed just above the upper divertor leg when a boron powder is dropped from the actual position on the upper port. The four candidate positions on the upper port are indicated in the upper-right of this figure as numbers enclosed by open circles, indicating that the toroidal angles of positions 1 and 2 and those of 3 and 4 are different. It should be noted that the shape of the poloidal cross-section of the LHD plasma at the two toroidal angles is different as shown in the lower part of this figure. While the plasma is vertically elongated at the toroidal angle of positions 1 and 2, it rotates counter-clockwise at positions 3 and 4.

Fig. 1 (a) shows the calculated trajectories of boron powders in four different plasma densities where the powders are dropped from just above the upper divertor legs underneath positions 1 and 2. The trajectories deviate from the plasma with the increase in the plasma density due to the effect of the plasma flow at the upper divertor legs. The calculations revealed that positions 1 and 2 are inappropriate for the installation because the boron powders do not reach the ergodic layer, especially for higher plasma densities. Fig. 1 (b) indicates the calculations where the boron powders dropped from positions 3 and 4, showing the trajectories are deflected at an upper divertor leg toward the outboard side of the torus, and the deflection is enhanced with the

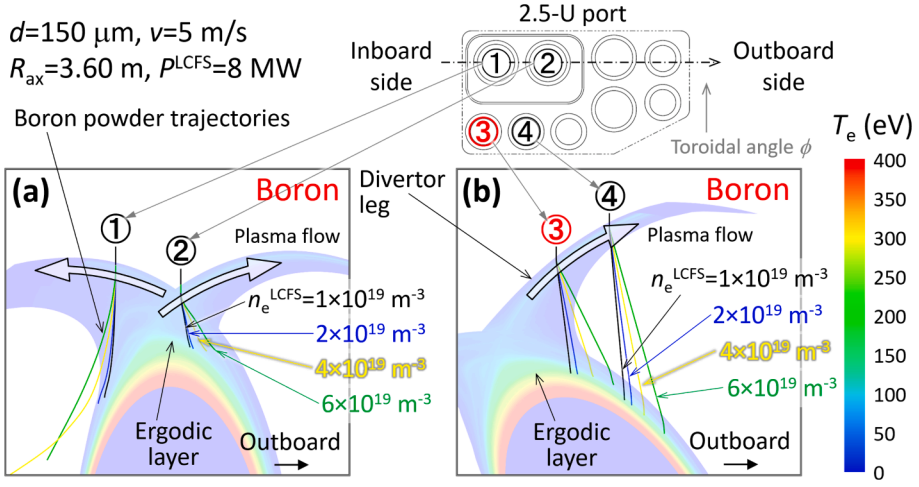

Fig. 1. The calculations of the trajectories of boron powders dropped from four candidate positions for the IPD on the upper port (2.5-U). The trajectories are indicated as colored lines for four plasma densities (n_e^{LCFS} = 1, 2, 4, and 6 × 10^{19} m^{-3}). The upper-right figure is a drawing of the top view of the upper port. The three-dimensional background plasma parameter profiles are provided by EMC3-EIRENE with a fixed plasma heating power (P^{LCFS} = 8 MW) for R_{ax} = 3.60 m. Figure (a) shows the calculated boron powder trajectories dropped from positions 1 and 2. Figure (b) indicates the calculated trajectories dropped from positions 3 and 4. The poloidal cross-sections of colored electron temperature profiles in the peripheral plasma for n_e^{LCFS} = 1 × 10^{19} m^{-3} and P^{LCFS} = 8 MW are illustrated to recognize the positional relationship between the trajectories and the plasma.

increase in the plasma density. The calculations show that the dropped powders penetrate the ergodic layer deeper than in positions 1 and 2. The simulations in Fig. 1 (b) demonstrate that the position in the inboard side of the torus is more advantageous for injecting the powders into the peripheral plasma (the ergodic layer) because of the deflection of the trajectory toward the outboard side for higher plasma densities. The simulations proposed that position 3 was optimum for installing the IPD for real-time boronization.

Analysis of the ablation positions of the dropped boron powders

As shown in Fig. 1, the plasma density affects the ablation positions of the dropped boron powders. For this reason, a systematic plasma density-scan experiment was performed to investigate the boron ion transport in the peripheral plasma during boron powder injection. Fig. 2 shows the time evolution of the representative plasma parameters in this experiment in which the radial position of the magnetic axis was $R_{ax} = 3.60$ m and the toroidal magnetic field was $B_t = 2.75$ Tesla. The direction of the toroidal magnetic field was clockwise when the torus was viewed from the top. The total port-through power of NBIs was estimated to be 14 MW which is output through the drift tube (not the power absorbed in the plasma). The line averaged plasma density, $\bar{n}_e$, was controlled to about 1, 2, 3, 4, and 5×10^{19} m^{-3} by feedback hydrogen gas fueling. It takes about 1 s for the boron powders to reach the peripheral plasma from the IPD. In this experiment, the powders reached the plasma at about 4 s and continued until about 5 s. The plasma parameters before and during the boron powder injection were almost the same because of a low powder drop rate of ~ 1 mg/s estimated by a reduction of laser intensity in a flowmeter installed in the IPD. While the radiation power, the intensity of H_α, the intensity of boron emission lines, and the stored energy increased with the plasma density, the central electron temperature decreased with the plasma density. Fig. 3 presents the radial profile of the electron temperature and density in three different line averaged plasma densities ($\bar{n}_e \sim 1$, 3, and 5×10^{19} m^{-3}) at 5.0 s (during boron powder injection), which were measured with a Thomson scattering system at a toroidal position where the plasma was horizontally elongated. The figure shows that the central electron temperature at a major radius R of about 3.6 m decreases with the plasma density.

The ablation position and distribution of the dropped boron powders were routinely monitored with a visible Charge Coupled Device (CCD) camera installed in an upper port close to the IPD [22]. Fig. 4 displays the images of the ablation of the boron powders in the three line averaged plasma densities ($\bar{n}_e \sim 1$, 3, and 5×10^{19} m^{-3}) at the initial phase of the powder injection, where the exposure time was set to 10 ms. Several stripes of visible light were observed during the powder injection, especially for the higher plasma densities. The boron powders were evaporated and released boron atoms into the plasma. The boron atoms were ionized and emitted visible light by interaction with the plasma. The boron ions moved along the magnetic field lines, producing the stripes of visible light. Fig. 4 shows that the main ablation area, where the stripes gathered with high brightness, was moved toward the outboard side of the torus with the increase in the plasma density, which also shows that the stripes dispersed toward the outboard side, especially for higher plasma densities.

The atomic boron source profile in the plasma is one of the critical parameters for the impurity transport simulation in the boron powder injection. The position and distribution of the boron source by the dropped boron powders in the plasma density-scan experiment were calculated using DUSTT. The profiles of plasma parameters were provided from the calculations by EMC3-EIRENE in which the plasma density inside the LCFS, n_e^{LCFS}, the plasma heating power inside the LCFS, P^{LCFS}, the perpendicular particle diffusion coefficient, $D_\perp$, and the electron/ion thermal diffusion coefficients, $\chi_{i,e\perp}$, were set to reproduce the observed electron density and temperature profiles in the peripheral plasma. The electron temperature and density profiles reproduced by EMC3-EIRENE in the plasma density scan experiment are indicated as small solid red circles and blue squares in Fig. 3, respectively. The above control parameters for reproducing the observed plasma parameter profiles for the three plasma densities are listed in Table 1.

Fig. 5 displays a perspective view of the three-dimensional model of the vacuum vessel and an LHD peripheral plasma in $R_{ax} = 3.60$ m for half of one helical section (18° in toroidal direction) which was made for the calculation of the trajectories and the ablation positions of dropped boron powders. The poloidal cross-sections of the plasma near the initial position are indicated as dark gray. Boron powders were dropped from the initial position just above the upper divertor leg underneath the optimized position (corresponding to position 3 in Fig. 1) with a downward velocity of 5 m/s. Using the loss rate of the powder's mass along the trajectories, the spatial distribution of the production rate of boron atoms evaporated from boron powders was calculated by DUSTT. A recent microscopic analysis revealed that the boron powders (a nominal diameter of 150 μm) used for the powder injection experiments

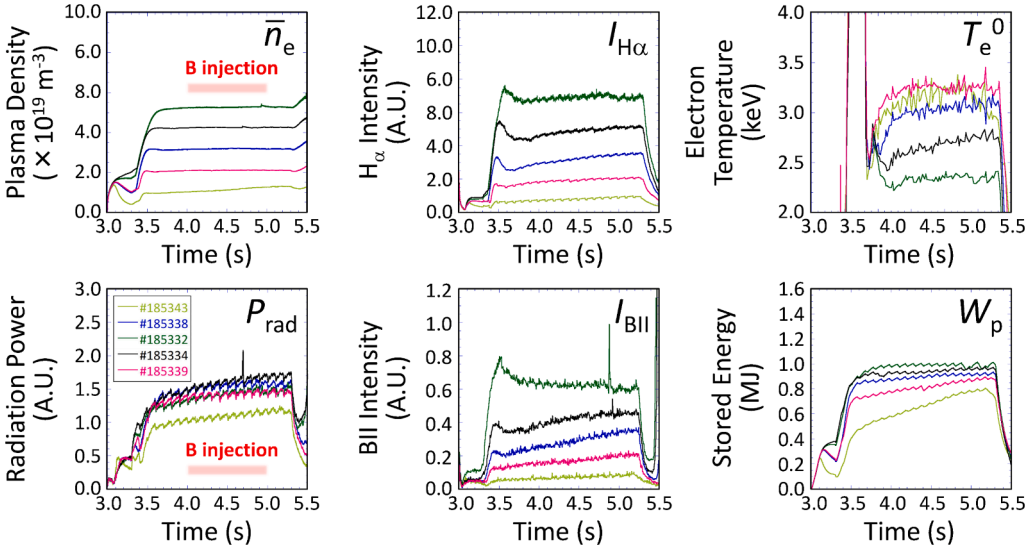

Fig. 2. The time traces of representative plasma parameters (line averaged plasma density, H_α intensity, central electron temperature, radiation power, BII intensity, and stored energy) in the plasma density-scan experiment with boron powder injection for $R_{ax} = 3.60$ m. The powders reached the peripheral plasma at about 4 s and continued until about 5 s.

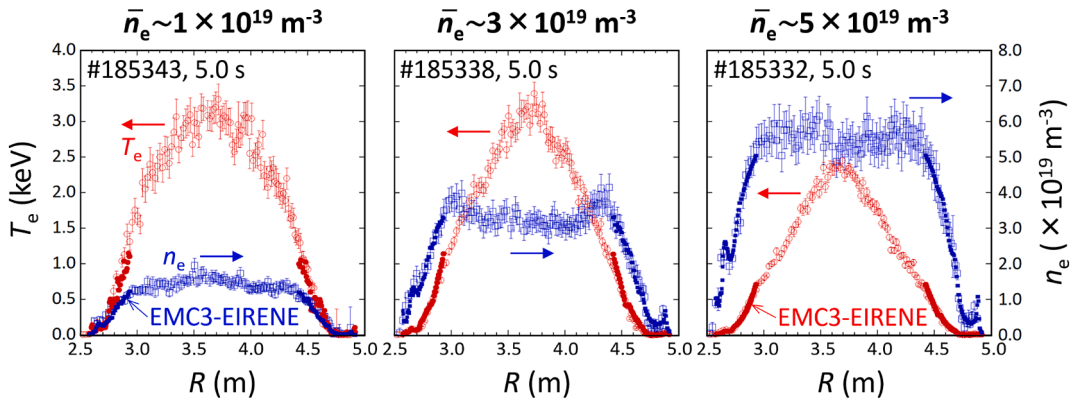

Fig. 3. The radial profiles of the electron temperature and density at 5 s (during boron powder injection) for three different line averaged plasma densities at a toroidal position where the LHD plasma is horizontally elongated, which were measured in the density scan experiment. The electron temperature and density profiles in the peripheral region reproduced by EMC3-EIRENE are indicated as small solid red circles and blue squares, respectively. (For interpretation of the references to colour in this figure legend, the reader is referred to the web version of this article.)

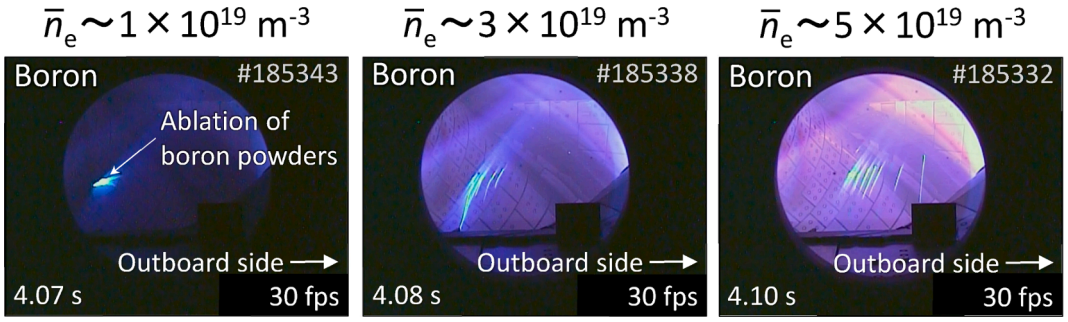

Fig. 4. The images of the ablation of dropped boron powders in three line averaged plasma densities ($\bar{n}_e$ = 1, 3, and 5 × 10^{19} m^{-3}) in the density-scan experiment, which were observed with a visible CCD camera installed in an upper port close to the IPD.

Table 1
A table showing the control parameters (the plasma density and the plasma heating power inside the LCFS, the perpendicular particle diffusion coefficient, and the electron/ion thermal diffusion coefficient) of EMC3-EIRENE for reproducing the measured radial profile of the plasma parameters in the density scan experiment shown in Fig. 3.

Shot No.	$\bar{n}_e$	n_e^{LCFS}	P^{LCFS}	$D_\perp$	$\chi_{i,e\perp}$
#185343	$\bar{n}_e \sim 1 \times 10^{19}$ m^{-3}	1.2×10^{19} m^{-3}	10.6 MW	0.7 m^2/s	0.023 m^2/s
#185338	$\bar{n}_e \sim 3 \times 10^{19}$ m^{-3}	3.4×10^{19} m^{-3}	12.2 MW	0.6 m^2/s	0.10 m^2/s
#185332	$\bar{n}_e \sim 5 \times 10^{19}$ m^{-3}	5.0×10^{19} m^{-3}	8.0 MW	0.4 m^2/s	0.26 m^2/s

have a size distribution, which found an average major axis length of the powders of about 107 μm with the full width at half maximum of 56 μm [23]. These parameters are newly implemented in DUSTT by dividing the size distribution into more than one hundred groups. The evaporated boron atoms are isotropically diffused with an energy corresponding to the evaporation temperature. Fig. 6 presents perspective views showing the distribution of the production rate of boron atoms in the peripheral plasma for the three line averaged plasma densities ($\bar{n}_e \sim 1$, 3, and 5 × 10^{19} m^{-3}), in which the production rate is expressed as colored spheres. The background plasma parameter profiles in the three line averaged plasma densities were calculated by EMC3-EIRENE in which the control parameters listed in Table 1 were used. The position of the framework in Fig. 6 corresponds to the area enclosed by a broken gray square in Fig. 5. The main ablation area of the boron powders is indicated as a group of red spheres, which shows that the position of the ablation area moves toward the outboard side with the increase in the plasma density. Fig. 6

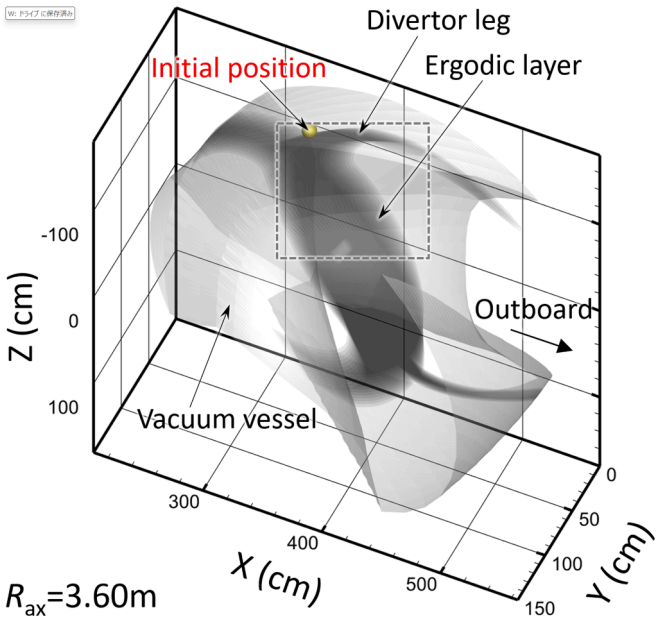

Fig. 5. A perspective view of a three-dimensional model of the vacuum vessel and the plasma for half of one helical section (18° in toroidal direction) to calculate the trajectories and ablation positions of dropped boron powders by the dust transport simulation. The poloidal cross-sections of the plasma near the initial position are indicated as dark gray inside the vacuum vessel.

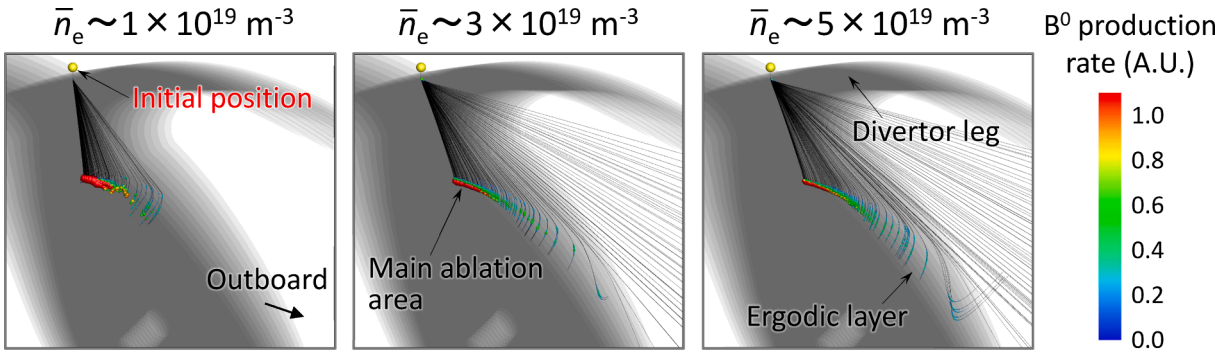

Fig. 6. The calculations of the distribution of the ablation positions of the dropped boron powders in the LHD peripheral plasma for three line averaged plasma densities ($\bar{n}_e$ = 1, 3, and 5 × 10^{19} m^{-3}), in which the background plasma parameter profiles are fitted to the measurements in the density-scan experiment. The production rate of boron atoms originating from dropped boron powders is indicated as colored spheres, and the trajectories of the dropped boron powders are shown as thin black lines. The position of the framework of these figures is shown as the broken gray square in Fig. 5.

also demonstrates that the distribution of the production rate disperses toward the outboard side, especially for higher plasma densities. The change in the position of the main ablation area is explained by the deflection of the trajectories of the dropped boron powders due to the effect of the plasma flow in the upper divertor leg. Smaller-sized boron powders are included in the dropped powders because of the size distribution. The plasma flow is more influential in dispersing the smaller-sized (lightweight) powders toward the outboard side, explaining the observed images of the ablation positions of the dropped boron powders in Fig. 4. The simulations showed that the ratio of the numbers of ionized boron atoms in the plasma to the total boron atoms contained in the dropped powders was 1.0, 0.85, and 0.76 for the three line averaged plasma densities, respectively. The negative dependence of the ionization ratio of the boron atoms on the plasma density indicates that smaller-sized boron powders are swept away by the plasma flow in the upper divertor leg, especially for higher plasma densities.

Full-torus impurity transport simulation during boron powder injection in the plasma density-scan experiment

Full-torus impurity transport simulation in the plasma density-scan experiment was performed to investigate spectroscopic measurements during the boron powder injection. The right figures in Fig. 7 are colored plots showing the time trend of the line-integrated intensity profile of two boron emission lines by B^0 and B$^+$ (BI (563.3 nm) and BII (494.0 nm), respectively) for a high line averaged plasma density of $\bar{n}_e \sim 5 \times 10^{19}$ m^{-3}, which was measured with a vertical visible spectrometer array installed in an outer port (10-O) [24,25]. The observations exhibited an increase in the intensity of the boron emission lines during the powder injection. On the left side of this figure, a poloidal cross-section of the vacuum vessel, the divertor plates, a dome, and an LHD plasma along the Line Of Sight (LOS) of the spectrometer array are illustrated. The cross-section of the radiation power density profile by B$^+$ calculated by EMC3-EIRENE is also shown. The code does not distinguish chemical and physical sputtering caused by the background hydrogen plasma. In this calculation, the sputtering rate of boron on the divertor plates was assumed to be 0.01 which is appropriate under typical plasma parameters on the divertor plates [26]. The self-sputtering of boron was not included because of the dominance of the hydrogen ion flux on the divertor plates. The simulation assumed a perpendicular diffusion coefficient of impurity (boron) ions of 1.0 m^2/s which is appropriate for reproducing both the observed line emission ratio of the outboard to the inboard side, and the absolute value of impurity (carbon) emission in LHD plasmas [27]. The simulation revealed that the total boron source from the divertor plates is much higher than that supplied by the IPD by around two orders of magnitude in this case. The observed intensity of the boron emission lines was high at the channels having LOS viewing the front of the divertor plates in the closed helical divertor region in the inboard side (around channel 28), indicating the sputtering of boron atoms on the divertor plates.

Fig. 8 (a) and (b) present the measured intensity profile of the two boron emission lines before and during the boron powder injection in the plasma density-scan experiment, respectively. The exposure time of the spectrometer was set to 50 ms. The measurements show that the

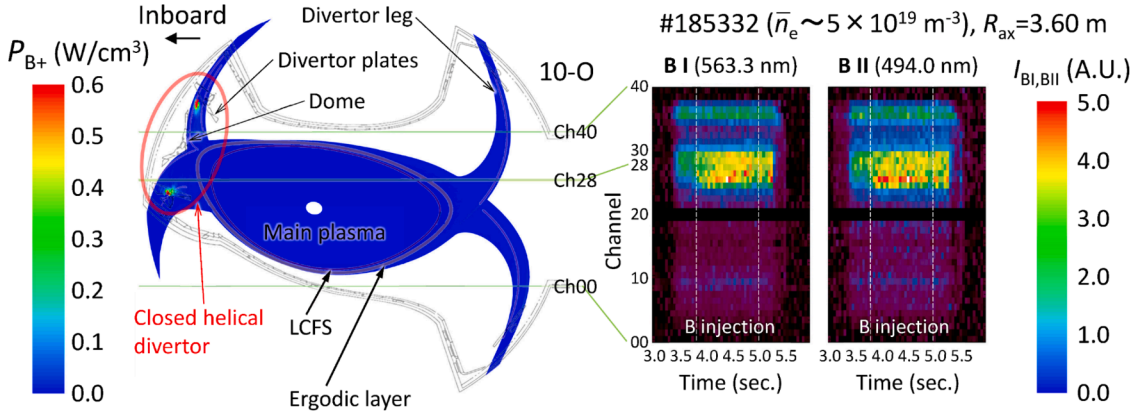

Fig. 7. The right figure presents the observed time evolution of the line-integrated intensity of two boron emission lines (BI (563.3 nm) and BII (494.0 nm)) for a high line averaged plasma density of 5 × 10^{19} m^{-3} in the plasma density-scan experiment. The left figure shows the poloidal cross-section of the vacuum vessel, divertor plates, dome, and LHD plasma along the LOS of the visible spectrometer array. The cross-section of the calculated radiation power density profile by singly ionized boron ions for the high plasma density is illustrated.

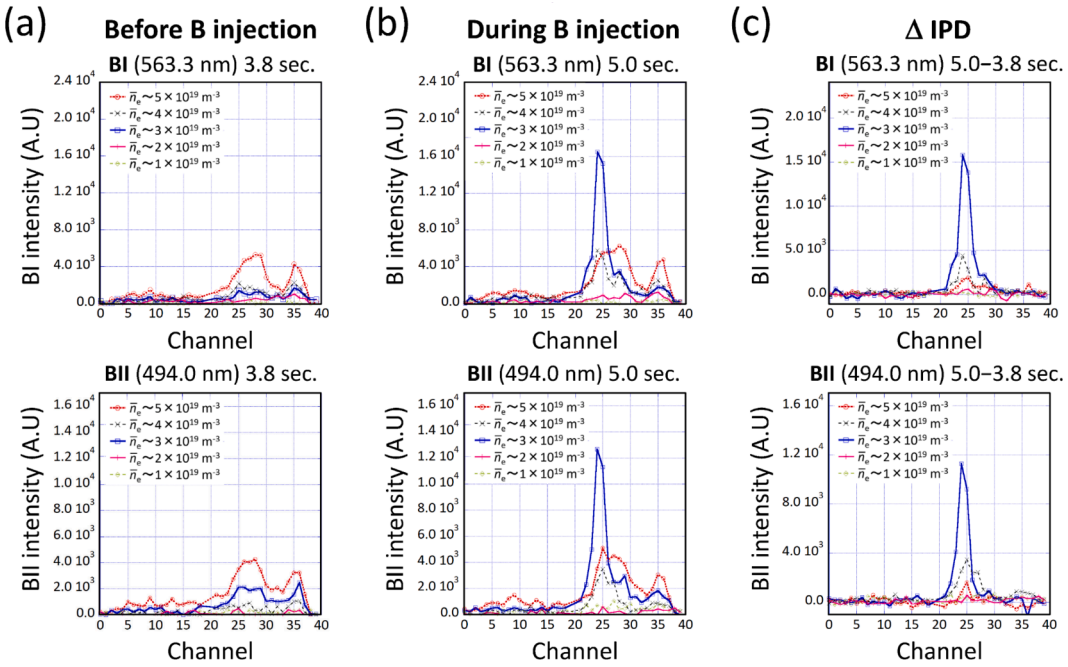

Fig. 8. The line-integrated intensity profiles of the two boron emission lines (BI (563.3 nm) and BII (494.0 nm)) before the boron powder injection (a) and during the injection (b), which were measured with the visible spectrometer array in the plasma density-scan experiment. The change in the intensity profiles of the boron emission lines is shown in Figure (c), which was obtained by subtracting the intensity profile during the injection from that before the injection.

intensities in lower line averaged plasma densities of $\bar{n}_e \sim 1 \times 10^{19}$ m^{-3} and 2×10^{19} m^{-3} were quite low, and the intensities around channels 25 and 36 were high for higher line averaged plasma densities, regardless of the powder injection. The high intensity around channel 36, viewing the top of the roof-shaped dome in the closed helical divertor region, cannot be explained by the simulation of the radiation power density profile shown in Fig. 7. One of the possible reasons for the high intensity could be unexpected PSI on the dome because the distance between the dome and the peripheral plasma is short (less than 10 mm). The unexpected PSI on the dome cannot be taken into account in the simulation, which disturbs the detailed analysis of the impurity transport in the boron powder injection experiment. For this reason, the perturbation method was applied to the analysis by subtracting the intensity profile before the powder injection from that during the injection, which extracts the increment of the intensity induced only by the boron powder injection. Fig. 8 (c) shows the extracted intensity profile which exhibits successful subtraction of the intensity of the boron emission lines around channel 36. The figure shows a large peak around channel 25 for a medium line averaged plasma density of $\bar{n}_e \sim 3 \times 10^{19}$ m^{-3}. It should be noted that the peak of the two boron emission lines (BI and BII) decreases with the increase in the plasma density.

The subtracted intensity profiles of the boron emission lines were investigated by a full-torus simulation using ERO2.0. Fig. 9 (a) illustrates the full-torus model for the simulation, in which EMC3-EIRENE provided the three-dimensional background plasma parameter profiles. The background plasmas were made by extending the simulations for one helical pitch angle (36° in toroidal direction) to the full-torus geometry under an assumption of helical symmetry. The calculations by DUSTT provided the distributions of the atomic boron source originating from the dropped boron powders, in which the drop rate was set to 1 mg/s. The initial position underneath the IPD is indicated as a yellow sphere, and the position of the LOS of the visible spectrometer array is illustrated as green lines. It should be noticed that the position of the spectrometer array is toroidally far from the IPD. In the ERO2.0 simulations, it was assumed that the plasma-facing side of all divertor plates consists of boron. The other parts such as the backside of the divertor plates, the dome, and the vacuum vessel were assumed to consist of carbon. To investigate the observations of the subtracted intensity profile of the boron emission lines, only the self-sputtering of boron induced by the dropped boron powders was considered (no sputtering of boron by the background hydrogen plasma was assumed). The reason for this assumption is that the subtracted intensity profiles consist of boron emission originating from the dropped boron powders. In this simulation, the boron atoms/ions originating from boron powders injected by the IPD, and boron atoms produced by the self-sputtering on the divertor plates induced by the injected boron powders are comprehensively taken into account. The dependence of the sputtering rate and the angular distribution of boron atoms on the incident angle and the energy of boron ions was derived from a database on plasma-wall interactions calculated by SDTrimSP [28]. Fig. 9 (b) presents the simulation of the full-torus density profile of neutral boron atoms evaporated from the dropped boron powders for the medium line averaged plasma density ($\bar{n}_e = 3 \times 10^{19}$ m^{-3}). The figure presents that the boron atoms are localized near the toroidal position where the IPD is installed. In this figure, the poloidal cross-sections of the boron density profile are displayed at the toroidal positions where the shape of the LHD plasma is horizontally or vertically elongated. In the ERO2.0 simulation, the trajectories of large amounts of test particles (about 40 million at maximum), which were representatives of boron atoms/ions in the plasma, were tracked in the full-torus model. Fig. 9 (c-f) exhibit the simulations of the density profile of boron ions with different charge states, showing that the boron ions toroidally transported with the increase in the charge state. The density of singly and doubly charged boron ions (B^+ and B^{2+}) was localized in the divertor region at the inboard side of the torus as shown in Fig. 9 (c) and (d).

Using the three-dimensional distribution of the plasma parameters and the calculated boron atom/ion densities, the profile of the radiation power density of the two boron emission lines was derived using an atomic-molecular database provided by ADAS [29]. Integrating the radiation power along the LOS of the spectrometer array provides the intensity profiles. Fig. 10 displays the simulations of the intensity profile for three line averaged plasma densities ($\bar{n}_e = 3$, 4, and 5×10^{19} m^{-3}). It shows that the peak value of the intensity for the higher plasma densities is larger than that for the medium plasma densities in both boron

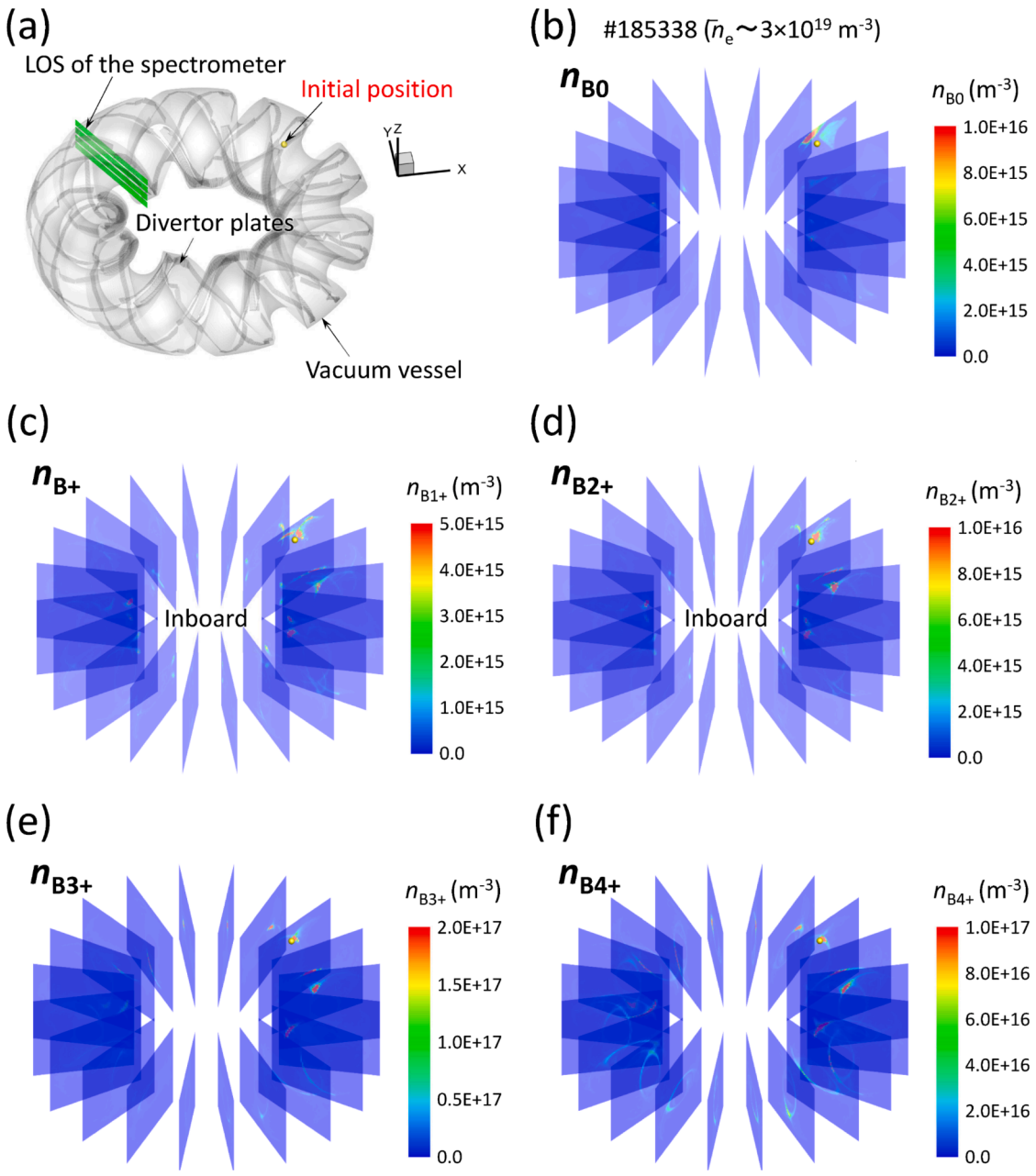

Fig. 9. (a) A perspective view of the full-torus model of the vacuum vessel and PFCs for the simulation. The LOS of the visible spectrometer array and the initial position of the boron powder injection underneath the IPD are indicated as green lines and a yellow sphere, respectively. (b) The simulation of the density profile of neutral boron atoms originating from the dropped boron powders for a medium line averaged plasma density of $\bar{n}_e = 3 \times 10^{19}$ m^{-3}. The three-dimensional background plasma parameter profile was provided by EMC3-EIRENE. (c-f) The simulations of the density profile of boron ions with different charge states (from B^+ to B^{4+}). The poloidal cross-sections at the toroidal angles where the shape of the plasma is horizontally or vertically elongated are displayed in the figures. (For interpretation of the references to colour in this figure legend, the reader is referred to the web version of this article.)

emission lines. Comparing the simulations with the observations shown in Fig. 8 (c), it was revealed that the simulation did not reproduce the observed decrease in the intensity with the increase in the plasma density. This discrepancy indicates that the assumption adopted in the ERO2.0 simulations in this analysis (the plasma-facing side of all divertor plates consists of boron) is not reasonable for reproducing the observations, which suggests a lower sputtering rate of boron on the divertor plates in the higher line averaged plasma densities. The observations of the lower intensity of the boron emission lines in the higher plasma densities can be explained by the lower density of boron deposited on the divertor plates at the LOS of the spectrometer. The previous full-torus simulation using ERO2.0 predicted a toroidally localized boron deposition near the IPD in a high plasma density and a toroidally uniform boron deposition in a low plasma density [21]. The experimental result suggesting the lower sputtering rate of boron is consistent with the previous full-torus simulations which indicated a lower boron density deposited on the divertor plates at the LOS of the spectrometer in the high plasma density. It has been found that the reason for the different toroidal distribution of the boron density in the low and high plasma densities is due to the difference in the connection lengths at the ablation positions of the dropped boron powders in the two different plasma densities [21].

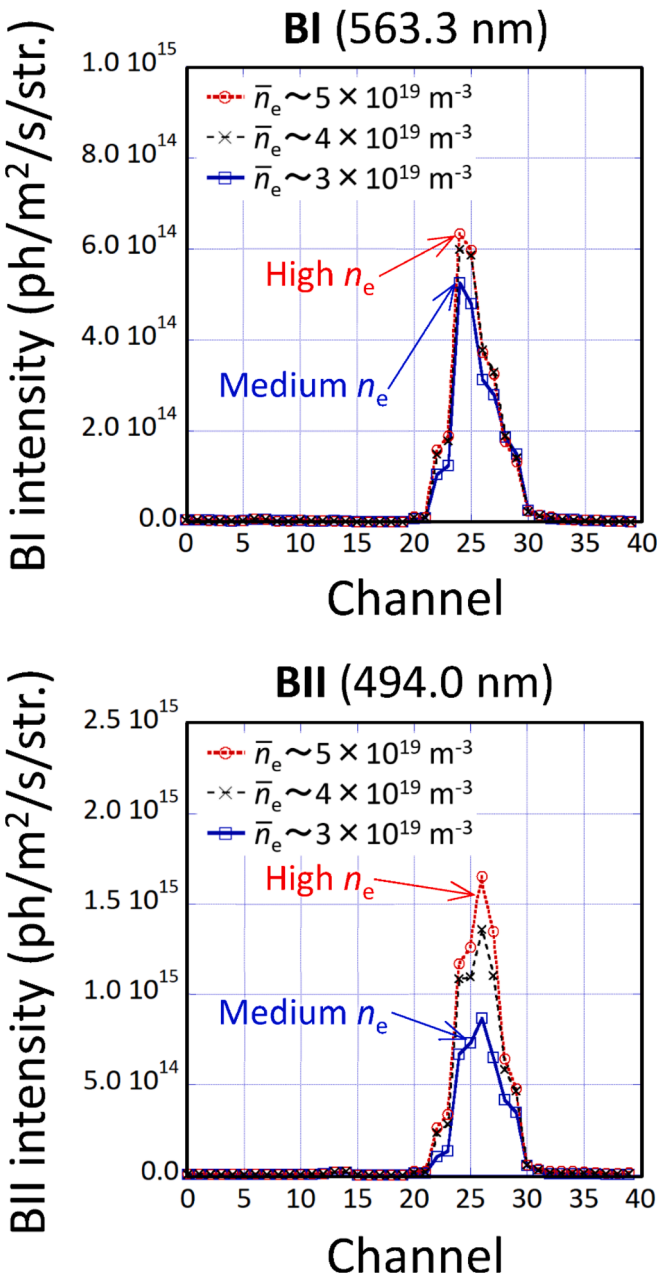

Fig. 10. Simulations of the line-integrated intensity profile of the two boron emission lines (BI (563.3 nm) and BII (494.0 nm)) along the LOS of the visible spectrometer array for three line averaged plasma densities ($\bar{n}_e$ = 3, 4, and 5 × 10^{19} m^{-3}), which were calculated by ERO2.0 using the full-torus model.

Summary

The calculations of dropped boron powder trajectories using DUSTT under three-dimensional background plasma parameter profiles by EMC3-EIRENE proposed an optimized position for installing the IPD for real-time boronization. It showed that the plasma density affects the dropped boron powder trajectories and the ablation positions in the peripheral plasma. A systematic plasma density-scan experiment was performed to investigate the toroidal distribution of the boron deposition on the PFCs by boron powder injection. A dust transport simulation proved that the main ablation area of the dropped boron powders changed toward the outboard side of the torus with the increase in plasma density. It also presented that the ablation positions dispersed toward the outboard side, especially for higher plasma densities, which was consistent with the observed images of the ablation of the dropped boron powders. A visible spectrometer array measured the intensity profiles of two boron emission lines (BI and BII) before and during the boron powder injection. By subtracting the intensity profile before the injection from that during the injection, the change in the intensity profile caused by the boron powder injection was successfully extracted. The subtracted intensity profiles in the plasma density-scan experiment were investigated by ERO2.0 using a full-torus model, showing that the simulation did not reproduce the observed decrease in the intensity of the boron emission lines for higher plasma densities. This discrepancy indicates a lower boron deposition density on the divertor plates at the LOS of the spectrometer array for the higher plasma densities. The position of the spectrometer array is toroidally far from the IPD. Thus, this result experimentally verifies the previous full-torus simulation showing a toroidally localized boron deposition adjacent to the IPD for the higher plasma densities.

CRediT authorship contribution statement

M. Shoji: Writing – original draft, Visualization, Validation, Software, Resources, Methodology, Investigation, Funding acquisition, Formal analysis, Data curation, Conceptualization. **G. Kawamura:** Software. **R. Smirnov:** Software. **J. Romazanov:** Software. **A. Kirschner:** Software. **Y. Tanaka:** Software. **S. Masuzaki:** Supervision, Project administration. **T. Kawate:** Resources, Data curation. **F. Nespoli:** Resources. **R. Lunsford:** Resources, Methodology. **E.P. Gilson:** Methodology. **S. Brezinsek:** Software. **N.A. Pablant:** Supervision, Resources.

Declaration of competing interest

The authors declare that they have no known competing financial interests or personal relationships that could have appeared to influence the work reported in this paper.

Acknowledgements

This work was performed under the auspices of the NIFS Collaboration Research program (NIFS22KIST004). One of the authors (M. S.) would like to thank Y. Feng for permission to use EMC3-EIRENE. He is also grateful for the computational resources of the plasma simulator in NIFS. This work is supported by a JSPS KAKENHI Grant Number 21K18620. This work is also supported by the U.S. Department Of Energy under Contract No. DE-AC02-09CH11466 with Princeton University. One of the authors (R. S.) acknowledges support by the U.S. Department of Energy, Office of Science, Office of Fusion Energy Sciences under Award No. DE-FG02-06ER54852.

Data availability statement

The LHD data can be accessed from the LHD data repository at https://www-lhd.nifs.ac.jp/pub/Repository_en.html.

Data availability

Data will be made available on request.

References

[1] A. Nagy, et al., Rev. Sci. Instrum. 89 (2018) 10K121.
[2] R. Lunsford, et al., Nucl. Fusion 59 (2019) 126034.
[3] A. Bortolon, et al., Nucl. Fusion 60 (2020) 126010.
[4] R. Lunsford, et al., Phys. Plasmas 28 (2021) 082506.
[5] R. Lunsford, et al., Nucl. Fusion 62 (2022) 086021.
[6] J. Winter, et al., Plasma Phys. Control. Fusion 38 (9) (1996) 1503.
[7] K. Nishimura, et al., J. Nucl. Mater. 337 (2005) 431.
[8] Y. Takeiri, et al., Nucl. Fusion 57 (2017) 102023.
[9] N. Federico, et al., Nucl. Mater. Energy 25 (2020) 10842.
[10] A.Y. Pigarov, et al., Phys. Plasmas 12 (2005) 122508.

[11] R.D. Smirnov, et al., Plasma Phys. Controlled Fusion 49 (2007) 347.
[12] Y. Tanaka, et al., J. Nucl. Mater. 415 (2011) S1106.
[13] Y. Feng, et al., Plasma Phys. Controlled Fusion 44 (2002) 611.
[14] Y. Feng, et al., Contrib. Plasma Phys. 54 (2014) 426.
[15] G. Kawamura, et al., Contrib. Plasma Phys. 54 (2014) 437.
[16] D. Reiter, et al., Fusion Sci. Technol. 47 (2005) 172.
[17] M. Shoji, et al., Contrib. Plasma Phys. 60 (2020) e201900101.
[18] N. Federico, et al., Nat. Phys. 18 (2022) 350–356.
[19] J. Romazanov, et al., Nucl. Mater. Energy 18 (2019) 331.
[20] J. Romazanov, et al., Nucl. Fusion 62 (2022) 036011.
[21] M. Shoji, et al., Nucl. Mater. Energy 25 (2020) 100853.
[22] M. Shoji, et al., Plasma Fusion Res. 15 (2020) 2402039.
[23] S. Sawford *et al.*, 65th Annual Meeting of the APS (2023), CP11.00123.
[24] M. Goto, et al., Fusion Sci. Technol. 58 (2010) 394.
[25] T. Kawate, et al., Nucl. Fusion 62 (2022) 126052.
[26] S. Masuzaki, et al., Nucl. Fusion 42 (2002) 750.
[27] S. Dai, et al., Nucl. Fusion 56 (2016) 066005.
[28] W. Möller, et al., Comput. Phys. Commun. 51 (1988) 355.
[29] The ADAS User Manual (version 2.6) https://www.adas.ac.uk/ (2004).